4-12-2023

The spin polarization of palladium on magneto-electric Cr_2O_3

Takashi Komesu

Will Echtenkamp,

Christian H. Binek

Peter A. Dowben

Journal of Physics: Condensed Matter

The spin polarization of palladium on magneto-electric Cr_2O_3

OPEN ACCESS
IOP Publishing
Journal of Physics: Condensed Matter
J. Phys.: Condens. Matter **35** (2023) 275801 (8pp)
https://doi.org/10.1088/1361-648X/acc710

The spin polarization of palladium on magneto-electric Cr_2O_3

Takashi Komesu*, Will Echtenkamp, Christian Binek and Peter A Dowben

Department of Physics and Astronomy and the Nebraska Center for Materials and Nanoscience, University of Nebraska-Lincoln, Jorgensen Hall 855 North 16th Street, Lincoln, NE 68588-0299, United States of America

E-mail: tkomesu2@unl.edu

Received 5 December 2022, revised 28 February 2023
Accepted for publication 23 March 2023
Published 12 April 2023

Abstract

While induced spin polarization of a palladium (Pd) overlayer on antiferromagnetic and magneto-electric $Cr_2O_3(0001)$ is possible because of the boundary polarization at the $Cr_2O_3(0001)$, in the single domain state, the Pd thin film appears to be ferromagnetic on its own, likely as a result of strain. In the conduction band, we find the experimental evidence of ferromagnetic spin polarized in Pd thin films on a $Cr_2O_3(0001)$ single crystal, especially in the thin limit, Pd thickness of around 1–4 nm. Indeed there is significant spin polarization in 10 Å thick Pd films on $Cr_2O_3(0001)$ at 310 K, i.e. above the Néel temperature of bulk Cr_2O_3. While $Cr_2O_3(0001)$ has surface moments that tend to align along the surface normal, for Pd on Cr_2O_3, the spin polarization contains an in-plane component. Strain in the Pd adlayer on $Cr_2O_3(0001)$ appears correlated to the spin polarization measured in spin polarized inverse photoemission spectroscopy. Further evidence for magnetization of Pd on Cr_2O_3 is provided by measurement of the exchange bias fields in Cr_2O_3/Pd(buffer)/$[Co/Pd]_n$ exchange bias systems. The magnitude of the exchange bias field is, over a wide temperature range, virtually unaffected by the Pd thickness variation between 1 and 2 nm.

Keywords: magneto-electric material, spin polarized electronic structure, spin polarized inverse photoemission spectroscopy

(Some figures may appear in colour only in the online journal)

1. Introduction

The boundary polarization, especially as the surface/interface, has been regarded as essential to the successful magneto-electric devices fabricated using chromia $Cr_2O_3(0001)$ [1–24]. This boundary spin polarization at the surface of $Cr_2O_3(0001)$ was predicted independently by Andreev [25] and Belashchenko [26] and has been experimentally verified by a variety of approaches [27–33] including spin polarized inverse photoemission (SPIPES) [28]. These SPIPES studies [34, 35] have been extended to boron doped chromia that retains a much higher Néel temperature as well as persistent surface polarization, although more canted off the surface normal than undoped chromia. At issue is whether the surface or boundary spin polarization of chromia $Cr_2O_3(0001)$ induces spin polarization in the palladium (Pd) adlayer or is the Pd adlayer ferromagnetic.

Induced polarization across a ferromagnetic/paramagnetic interface is known and can be understood in the context of the Landau–Ginzburg equation [36–42], a mean field model without a microscopic Hamiltonian. This approach has been applied to ferromagnetic layers adjacent to Pd [36–39]. While chromia is not ferromagnetic, the boundary spin polarization

* Author to whom any correspondence should be addressed.

should play a similar role [32]. On the other hand, strained Pd layers have been observed to be ferromagnetic [43–46]. Pd layers on chromia are certainly strained. This dichomety would have a profound effect on the mechanism for exchange bias in Cr_2O_3/Pd/[Pd/Co]$_n$ structure [27, 29, 47, 48].

Pd, as a heavy metal similar to Pt, is often used in Hall-bar structures to read out the magnetic state of an adjacent magnetic layer [27, 49–54]. The read-out mechanism is widely considered to be the spin Hall magnetoresistance effect, which originates from a combination of the spin Hall and inverse spin Hall effects. The spin Hall effect in turn gives rise to a family of spin Hall effect devices [55, 56] and heavy metal Hall bars have been utilized in many spintronic device proposals. The presence of magnetization in the sensor layer, however, affects the Hall signal and has thus important implications for the interpretation of the measured signal. For example, the presence of intrinsic magnetization in the Pd sensing layer will give rise to a contribution to the Hall signal which does not originate from spin Hall magnetoresistance but rather anomalous Hall effect. Therefore, it is important to know and investigate how strain in Pd films can give rise to magnetization.

We have investigated Pd on magneto-electric chromia, $Cr_2O_3(0001)$, using spin SPIPES, as well as spin polarized photoemission, but here there is an emphasis on the spin polarization determined by SPIPES, because inverse photoemission is extremely surface sensitive [57, 58]. The experimental evidence points to ferromagnetism in Pd overlayers on $Cr_2O_3(0001)$ and that Pd on $Cr_2O_3(0001)$ is more than just a paramagnet with an induced polarization arising from the chromia boundary polarization.

2. Experimental

We have investigated Pd adlayers on single crystal of $Cr_2O_3(0001)$. The clean $Cr_2O_3(0001)$ single crystal was prepared by Ar^+ ions sputtering, with 1.5 keV in 2×10^{-5} Torr of Ar gas pressure, typically for 60 min at a sample emission current of about 6 μA. The $Cr_2O_3(0001)$ single crystal was subsequently annealed in oxygen (O_2) gas pressure, 8×10^{-8} Torr for about 20 min, to 1000 K, for several cycles, to obtain an ordered surface with no O_2 vacancies. X-ray photoemission spectroscopy (XPS) was used to confirm a contamination free surface while low energy electron diffraction (LEED) measurements was used to establish the crystallographic order of the single crystal $Cr_2O_3(0001)$ and the Pd overlayer. The lattice constant of the Pd adlayer was extracted from the LEED measurements. The reduction of oxygen vacancies contributed to the insulating character of the $Cr_2O_3(0001)$ single crystal surface and this in turn leads to an XPS core level shift to higher binding energies, after annealing with O_2, as expected [59–66]. The Pd adlayers were grown through Pd evaporation, via e-beam bombardment of a crucible, at a deposition rate of about 1 min $Å^{-1}$ and film thickness determined with a film thickness monitor and confirmed by XPS in the thin film limit.

The SPIPES experiments were carried out with a transversely polarized spin electron gun based on a prior Ciccacci design [67], as described elsewhere [68, 69]. The spin polarized electron gun used a GaAs single crystal as the spin polarized electron source 'activated' (with O_2 and cesium alternative deposition) in a separate chamber, with the initial photocurrent circular generated by circularly polarized laser beam. The spin polarized electron source was designed to be vacuum continuous with the spectrometer chamber equipped with an iodine-based Geiger–Müller isochromat photon detector described some details else where [69]. This SPIPES system is designed so that the incident spin polarization direction is transverse (perpendicular) with respect to the incident electron momentum and parallel (or antiparallel) with the applied field for all sample angles, to maximize our spin-sensitivity. There are 2 different modes for investigation of the boundary spin polarization, with the SPIPES system, whose value depends on the magnetic characteristics of the sample. In determining surface in-plane spin polarization of 'ferromagnetic materials' an external pulsed magnetic field, of about 400 Oe, is applied to the sample prior in one direction then the spin polarized inverse spectrum taken for that magnetization direction at remanence. Then the direction of pulsed external magnetic field is reversed and then the spin polarized inverse spectrum taken for the opposite magnetization direction at remanence. In this mode, incident electron spin direction as spin polarized electron is fixed. Because we have used $Cr_2O_3(0001)$ single crystal, not a thin film where parasitic magnetization can interact with an applied magnetic field giving rise to a magnetically selected single domain state [70], the 400 Oe pulse field is an insufficient field to reverse the antiferromagnetic spin configuration in the bulk. As a result, the net spin polarization was determined by switching of polarization direction of incident spin polarized electrons with reversal of the circular polarized light helicity used to general the spin polarized photocurrent. This results in reversal of the outgoing spin polarized electron spin direction. SPIPES is characterized by low count rates, so many sets of data are averaged together for each spectrum shown here in this work, as is typical of SPIPES. The spectra were obtained at remanence with the electron incidence along the surface normal and the energy resolution was approximately 400 meV. Typical of such instruments, the electron gun spin-polarization is 28%. As is typical of SPIPES, all spin-resolved spectra have been renormalized to a 100% hypothetical beam polarization. Instrumental asymmetries in SPIPES have been checked and removed by alternating the magnetic field after each sweep of electron gun energy. The Fermi level was established from tantalum or gold in electrical contact with the sample for all the measurements described herein.

3. Spin polarization at room temperature

Room temperature (294 K) is only slightly below the chromia Néel temperature (307 K), yet the exchange bias field, H_{EB}, in a chromia/Pd/(CoPd)n multilayer stack persists very close to the chromia Néel temperature, as seen in figure 1. The exchange bias field, H_{EB}, observed after isothermal switching through an applied magnetic field as seen in figure 1, has been seen before [27, 29, 48]. The magnitude of the exchange bias field changes with temperature, but remains nonzero at 294 K,

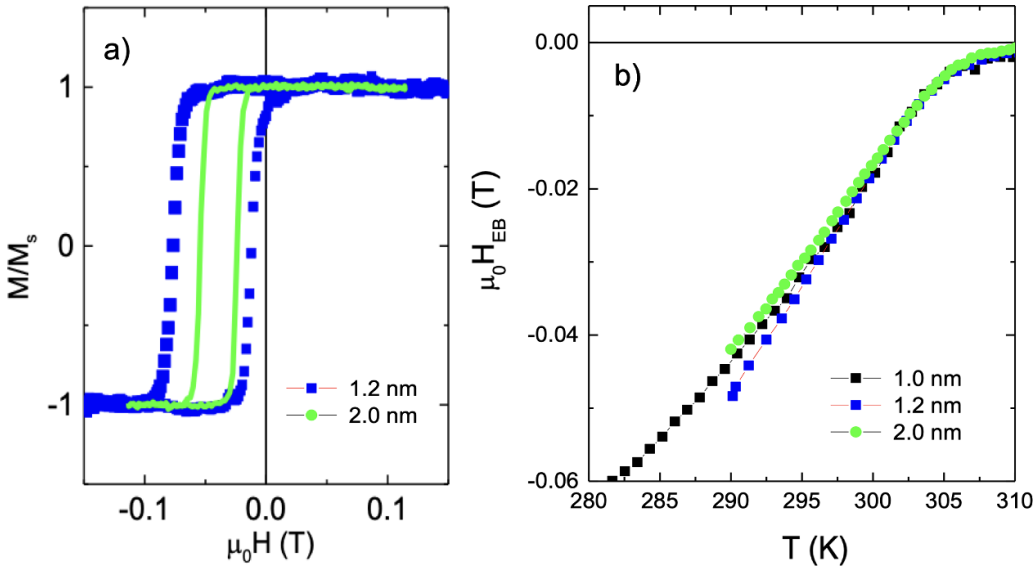

Figure 1. The temperature dependence of exchange bias in various chromia/Pd/(CoPd)$_n$ heterostructures with for Pd buffer layer thicknesses of 1.0, 1.2, and 2.0 nm. Typical exchange bias at 292 K, as a function of applied field for chromia/Pd/(CoPd)$_n$ heterostructures with for Pd buffer layer thicknesses of 1.2 (blue) and 2.0 nm (green) and (a) and the exchange bias plotted as function of temperature for chromia/Pd/(CoPd)$_n$ heterostructures with for Pd buffer layer thicknesses of 1.0 (black), 1.2 (blue), and 2.0 nm (green).

suggestive of a persistent boundary polarization at the interface between Pd and Cr_2O_3(001).

Most remarkably, on increasing the thickness of the Pd buffer layer separating the ferromagnetic Co/Pd multilayer from the antiferromagnetic pinning layer, one would expect an exponential decrease of the exchange bias with increasing buffer layer thickness [39]. Such a dependence or any significant dependence for the three buffer layer thicknesses of 1.0, 1.2 and 2.0 nm is not observed (see figure 1(b)). This indicates that the Pd layer does not behave as a nonmagnetic buffer layer but rather is magnetized and behaves as part of the overall ferromagnetic film.

For the SPIPES studies, the Cr_2O_3 sample was magnetoelectrically field cooled in applied *E* and *B* fields through the chromia Néel temperature (307 K), in order to put Cr_2O_3 in a single domain state and enhance the net surface polarization. Figure 2 shows the in-plane SPIPES of the unoccupied density of states for various thicknesses of the Pd overlayers deposited on top of Cr_2O_3. The in-plane SPIPES reveals some Pd spin projection parallel (SPIPES) to the film plane at 294 K temperature. Although the boundary spin polarization of chromia is generally regarded as along the surface normal, the canting this combination of measurements implies is not unusual and has been seen in previous measurement for Co on Cr_2O_3(0001) single crystals [71], while in-plane net polarization has been obtained for Cr_2O_3(0001) single crystals in SPIPES [28], as noted above.

The surface net spin polarization of the unoccupied Pd 4d-bands to 1 eV above the Fermi level retain net spin polarization with increasing Pd film thickness as is evident in the SPIPES spectra of figure 2. Figure 2 shows the SPIPES results as a function of the Pd layer thickness grown on a Cr_2O_3(0001) single crystal. The feature just above the Fermi level that increases with increasing Pd cover is associated with the unoccupied Pd d-band [72] and has been seen in prior inverse photoemission studies of Pd(111) [72, 73]. Since the spin majority does not align with spin minority, throughout the conduction band region, there is clearly net spin polarization, and the spin asymmetry is band dependent. As the Pd film thickness exceeds the ultra-thin film limit of 5 Å, the unoccupied Pd 4d band has majority spin polarization, as is evident in the SPIPES, as shown in figure 2. Because SPIPES is so surfaces sensitive, we can conclude that the net surface spin polarization of the Pd adlayer generally, and especially the spin asymmetry of the unoccupied Pd 4d-band, appears to decrease with increasing Pd film thickness, greater than 10 Å, as summarized in figure 3.

4. The correlation between strain and in-plane Pd layer surface polarization

The Pd adlayers grown on a Cr_2O_3(0001) single crystal are well ordered. The LEED shows that not only is the clean Cr_2O_3(0001) single crystal well ordered but that there is retention of surface order up to a Pd thickness of 120 Å deposited on a Cr_2O_3(0001) single crystal, as seen in figure 4. The clean Cr_2O_3(0001) single crystal gives the hcp type hexagonal pattern seen before in LEED [74–77], but because of the surface, the symmetry is known to be C_{3v} symmetry, i.e. three fold symmetry, not six fold.

A more subtle aspect of the Pd thin films deposited on a Cr_2O_3(0001) single crystal is that the Pd-Pd distance, as determined from LEED, is larger than the accepted in-plane Pd–Pd 2.751 Å spacing [78–80]. The maximum lattice expansion of Pd on Cr_2O_3(0001), from the analysis of the LEED, is about 14%–15% at a Pd layer thickness of about 1 nm (10 Å) on Cr_2O_3(0001). This expanded lattice constant in the thinnest

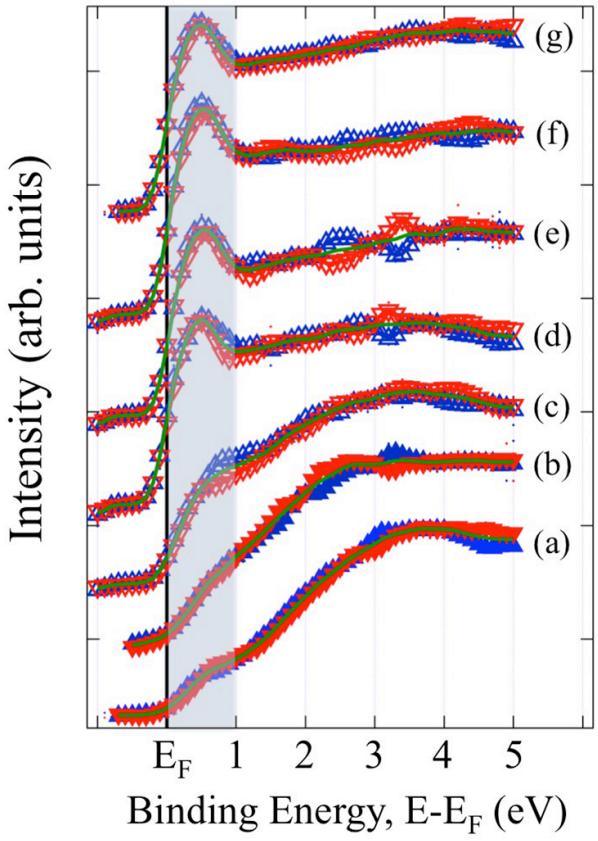

Figure 2. The spin polarized inverse photoemission spectroscopy (SPIPES) results as a function of (a) none, (b) 5 Å, (c) 10 Å, (d) 30 Å, (e) 40 Å, (f) 80 Å, and (g) 120 Å Pd layer thickness grown Cr_2O_3(0001) at 294 K. The blue upward triangles are for the spin up majority state and the red downward triangle is for spin down minority state. The green curve indicates the spin average. The unoccupied state binding energies given relative to the Fermi level (E-E_F). The spectra shown with filled symbols were taken by reversing the incident electron spin polarization direction, the rest of the spectra taken by reversing the pulse magnetic field.

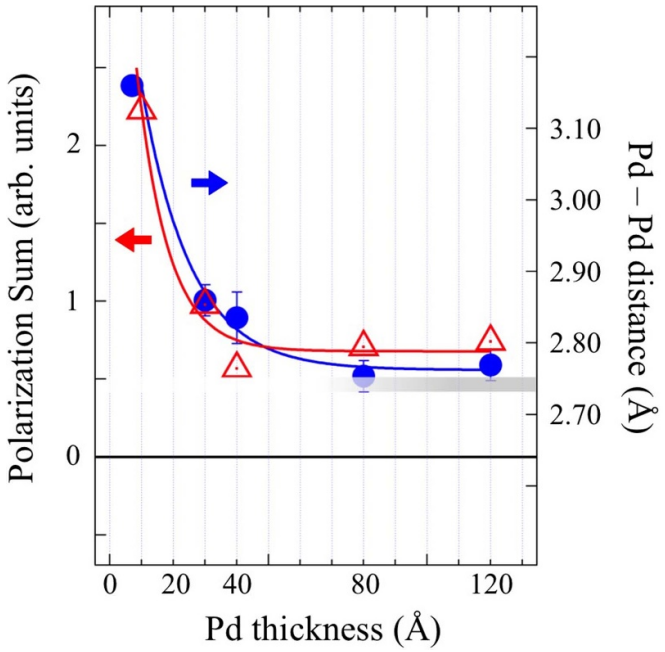

Figure 3. The summed spin polarization (red triangles) between the Fermi level (E_F) and 1 eV above the Fermi level, E-E_F, as determined from spin polarized inverse photoemission (figure 4) compared to the Pd–Pd distance (blue circles) as determined from low energy electron diffraction (LEED), shown in figure 6, both for Pd layers Cr_2O_3(0001) as a function of the Pd layer thickness. The in-plane Pd-Pd distance of bulk Pd(111) is indicated by the grey stripe.

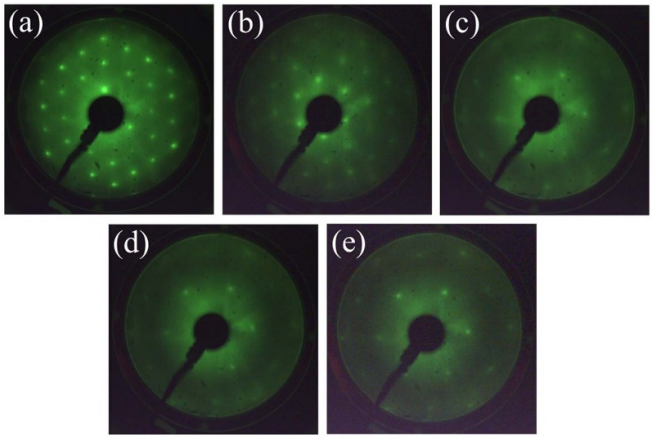

Figure 4. The low energy electron diffraction (LEED) patterns as a function of the Pd layer thickness grown Cr_2O_3(0001) at 294 K. The LEED diffraction shown are for Pd layer thicknesses on the clean Cr_2O_3(0001) of (a) clean Cr_2O_3(0001), (b) for 10 Å, (c) for 40 Å, (d) for 80 Å, (e) for 120 Å respectively. The electron energy was 230 eV for all images.

Pd films is larger than the 2.88 Å Pd–Pd spacing that would put the Pd layer in registry with the Cr_2O_3 surface as has been observed previously for Pd thin films on Cr_2O_3 [80]. At a film thickness of 2 to 4 nm, the measured in-plane Pd-Pd lattice constant does cluster about 2.88 Å, which is consistent with prior work [80], and places the Pd in registry with the Cr_2O_3 surface. As the Pd film thickness increases the LEED indicates that the Pd–Pd spacing decreases with increasing Pd adlayer film thickness on the Cr_2O_3(0001) substrate, as summarized in figure 4. Further deposition of Pd on Cr_2O_3(0001) leads to a relaxation of the expansive strain to relaxed value of bulk lattice constant of close to 3.89 Å [78, 79], or Pd–Pd distance of 2.75 Å [78–80]. Strain relief is very much expected for metal thin films with increasing film thickness [81].

By plotting the in-plane Pd–Pd lattice constant, determined from LEED, and the net spin polarization determined from SPIPES, as seen in figure 3. It is clear that both the in-plane Pd lattice constant from LEED and the spin polarization extracted from SPIPES follow very similar trends. As the Pd layer thickness on Cr_2O_3(0001) increases, the spin polarization that the surface of the Pd film decreases, but so does the lattice expansion measure in LEED. This suggests that the measured spin polarization is related to strain. Strain, however, is related to Pd thin film ferromagnetism [43–46, 82–85], as noted in the introduction. The expansive strain that appears to be associated to ferromagnetic Pd in prior work is about 1%–2% [45, 84], while here the expansion of the Pd thin film lattice is 15% for the thinnest Pd films and reducing to 2% at Pd film thicknesses of 80 Å.

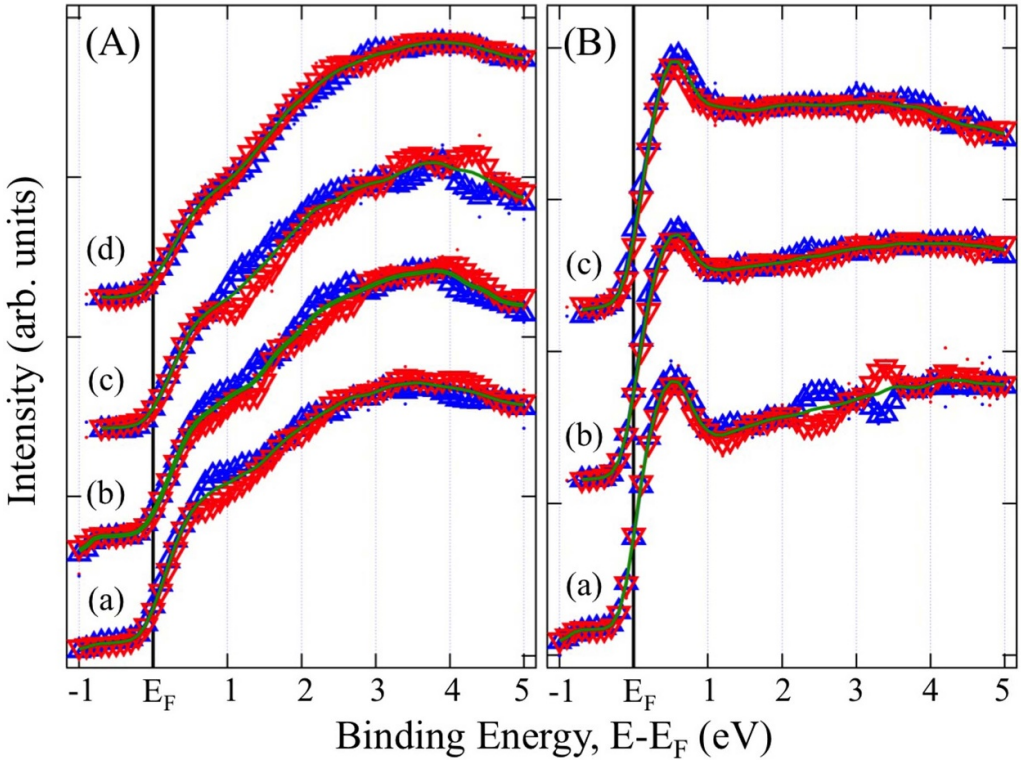

Figure 5. Evidence of net spin polarization of the unoccupied states for 10 Å (A) and 40 Å (B) thick Pd films on Cr_2O_3(0001), from spin polarized inverse photoemission. This temperature dependent SPIPES measurement of Pd thickness of 10 Å (A) and 40 Å (B) on Cr_2O_3 (0001) and summarized. For 10 Å thick Pd films on Cr_2O_3(0001) (A) the SPIPES spectra were taken at approximately (a) 294 K, i.e. room temperature, (b) 305 K, (c) 310 K, and (d) 470 K. For 40 Å thick Pd films on Cr_2O_3(0001) (B) the SPIPES spectra were taken at approximately (a) 294 K, i.e. room temperature, (b) 330 K, and (c) 470 K.

5. Ferromagnetic Pd thin films on Cr_2O_3(0001)

The weight of the evidence indicates that Pd layers less than 80 Å to 120 Å thick are ferromagnetic on Cr_2O_3(0001). There are several indicators that all point to a ferromagnetic Pd layer Cr_2O_3(0001).

The Landau–Ginzburg mean field approach in describing the induced polarization in a paramagnet on a ferromagnet would have induced magnetization decay decays as $M(z) = Re^{-kz}$ where z is the distance from the paramagnet/ferromagnet interface and k^{-1} is the paramagnetic correlation length [40–42, 86]. Cr_2O_3 is, of course not a ferromagnet, but an antiferromagnetic, but it is a magneto-electric and the Cr_2O_3(0001) surface exhibits a spin polarized boundary layer in the single domain state [27–33], often referred (incorrectly) as a magnetic surface layer. The boundary between the spin-polarized layer of Cr_2O_3(0001) and a Pd overlayer does exhibit the push-pull of magnetization across the boundary that is reminiscent of the Landau–Ginzburg mean field approach [32], Landau–Ginzburg mean field approach does not apply. While the spin polarization Pd adlayer, measured from SPIPES, does appear to decrease roughly as an exponential with the increasing Pd film thickness on Cr_2O_3(0001), as plotted in figure 3, the spin polarization does not go to zero as would be expected for induced polarization in a paramagnet. But the Pd-Pd in-plane strain, determined from LEED, has not gone to zero at a Pd film thickness of 80 Å on Cr_2O_3(0001). This persistent spin polarization is consistent with the observation that exchange coupling in chromia/Pd/$(CoPd)_n$ heterostructures, as seen in figure 1, remains little perturbed as the Pd buffer layer thicknesses is increased from 10 Å, to 12 Å and then to 20 Å. Here again, in the simple picture from Landau-Ginzburg, we would expect an exponential decay if the Pd adlayer is paramagnetic, which is not seen.

Because there is a measure net spin polarization at remanence with a rough 400 Oe pulsed magnetic field (figure 2) which is too small an applied field to reverse the domain state of a chromia single crystal [70], this implies that there is a reversal of the remnant polarization of the Pd adlayer.

Perhaps most compelling is that the Pd layer on Cr_2O_3(0001) retains net spin polarization in SPIPES, at temperatures above the Néel temperature of chromia (307 K), as seen in figure 5. Again, since the spin majority does not align with spin minority, throughout the conduction band region, there is clearly net spin polarization, and the spin asymmetry is band dependent. This is clear for the feature just above the Fermi level for the 40 Å thick Pd films on Cr_2O_3(0001) (figure 5(b)) and in the region of 1–3 eV above the Fermi level for 10 Å thick Pd films on Cr_2O_3(0001) (figure 5(a)). For chromia, Cr_2O_3(0001), the spin polarization is lost above the Néel temperature [27, 28]. The general trend is that the net spin polarization decreases with increasing temperature, but significant spin polarization is seen at 310 K for 10 Å thick Pd films on Cr_2O_3(0001), where in fact there should be none.

6. Summary

We have performed spin polarized electronic structure investigations of Pd overlayers grown on Cr_2O_3(0001) single crystal. All-in-all, the data cannot be reconciled with a paramagnetic Pd layer on Cr_2O_3(0001) where the spin polarization is due solely to the induced polarization arising from the uncompensated spins at the Cr_2O_3(0001) surface. We cannot exclude the induced polarization contributes to the net polarization of the ferromagnetic Pd adlayer, but this cannot fully explain the spin polarization of the Pd adlayer above the Neel temperature of chromia nor the exchange coupling effects seen.

The LEED indicates that significant expansive strain occurs in the 10 Å to 40 Å, 1–4 nm, thick Pd(111) layers Cr_2O_3(0001). As in other work [43–46, 70–73], strain is implicated as contributing to the ferromagnetism in the Pd film. We note that here the ferromagnetism is in Pd(111) while in prior work the films are textured along Pd(001).

Data availability statement

All data that support the findings of this study are included within the article (and any supplementary files).

Acknowledgments

This research was supported by the National Science Foundation through the EPSCoR RII Track-1: Emergent Quantum Materials and Technologies (EQUATE), Award OIA-2044049; the Nebraska Materials Research Science and Engineering Center Grant No. DMR-1420645; and the Nebraska Nanoscale Facility: National Nanotechnology Coordinated Infrastructure and the Nebraska Center for Materials and Nanoscience, under Award ECCS: 2025298, and nCORE, a wholly owned subsidiary of the Semiconductor Research Corporation (SRC), through the Center on Antiferromagnetic Magneto-electric Memory and Logic tasks #2760.00 and #2760.002 and NSF through ECCS 1740136. The authors would like to thank Prescott Evans for his assistance with the spin polarized photoemission.

ORCID iDs

Takashi Komesu https://orcid.org/0000-0002-2826-4193
Christian Binek https://orcid.org/0000-0002-0026-0772
Peter A Dowben https://orcid.org/0000-0002-2198-4710

References

[1] Binek C and Doudin B 2005 Magnetoelectronics with magnetoelectrics *J. Phys.: Condens. Matter* **17** L39–44
[2] Chen X, Hochstrat A, Borisov P and Kleemann W 2006 Magnetoelectric exchange bias systems in spintronics *Appl. Phys. Lett.* **89** 202508
[3] Sharma N, Marshall A, Bird J P and Dowben P A 2015 Magneto-electric magnetic tunnel junction as process adder for non-volatile memory applications *Proc. On IEEE Xplore; Circuits and Systems Conf. (DCAS)* (IEEE Dallas) pp 978-1-4673-7980-9/15
[4] Sharma N, Marshall A, Bird J and Dowben P A 2016 Multi-bit adder design using the compact model of the ME-MTJ device and its derived structures *The 11th Int. Conf. on Advanced Semiconductor Devices and Microsystems (ASDAM)* (IEEE Xplore) 16580073 pp 89–92
[5] Sharma N, Marshall A, Bird J and Dowben P A 2016 VerilogA based compact model of a three-terminal ME-MTJ device *Proc. 16th Int. Conf. on Nanotechnology* (Sendai: IEEE Xplore) 16498661 pp 145–8
[6] Sharma N, Marshall A, Bird J and Dowben P A 2015 Magneto-electric magnetic tunnel junction logic devices *4th Berkeley Symp. on Energy Efficient Electronic Systems (E3S)* (IEEE Xplore)
[7] Ahmed R and Victora R H 2018 A fully electric field driven scalable magnetoelectric switching element *Appl. Phys. Lett.* **112** 182401
[8] Dowben P A, Binek C and Nikonov D E 2016 Potential of nonvolatile magnetoelectric devices for spintronic applications *Nanoscale Silicon Devices* ed S Oda, D Ferry and T Francis (London) ch 11, pp 255–78
[9] Pan C and Naeemi A 2018 An expanded benchmarking of beyond-CMOS devices based on boolean and neuromorphic representative circuits *IEEE J. Explor. Solid-State Comput. Devices Circuits* **3** 101–10
[10] Sharma N, Bird J P, Binek C H, Dowben P A, Nikonov D and Marshall A 2020 Evolving magneto-electric device technologies *Semicond. Sci. Technol.* **35** 073001
[11] Nikonov D E and Young I A 2013 Overview of beyond-CMOS devices and a uniform methodology for their benchmarking *Proc. IEEE* **101** 2498–533
[12] Nikonov D E and Young I A 2014 Benchmarking spintronic logic devices based on magnetoelectric oxides *J. Mater. Res.* **29** 2109–15
[13] Dowben P A, Binek C, Zhang K, Wang L, Mei W-N, Bird J P, Singisetti U, Hong X, Wang K L and Nikonov D 2018 Towards a strong spin-orbit coupling magnetoelectric transistor *IEEE J. Explor. Solid-State Comput. Devices Circuits* **4** 1–9
[14] Sharma N, Marshall A, Bird J P and Dowben P A 2017 Verilog-A based compact modeling of the ME-FET device *5th Berkeley Symp. on Symp. & Steep Transistors Workshop (E3S)* (IEEE Xplore) (available at: https://ieeexplore.ieee.org/document/8246186)
[15] Sharma N, Binek C, Marshall A, Bird J P, Dowben P A and Nikonov D 2018 Compact modeling and design of magneto-electric transistor devices and circuits *31st IEEE Int. System-on-Chip Conf. (SOCC)* (Arlington, VA: IEEE Xplore) pp 146–51 (available at: https://ieeexplore.ieee.org/document/8618494)
[16] Pan C and Naeemi A 2018 Complementary logic implementation for antiferromagnet field-effect transistors *IEEE J. Explor. Solid-State Comput. Devices Circuits* **4** 69–75
[17] He K *et al* 2022 Graphene on chromia: a system for beyond-room-temperature spintronics *Adv. Mater.* **34** 2105023
[18] Choudhary R, Kumar P, Manchanda P, Sellmyer D J, Dowben P A, Kashyap A and Skomski R 2016 Interface-induced spin polarization in graphene on chromia *IEEE Magn. Lett.* **7** 3101604
[19] Cao S, Xiao Z, Kwan C-P, Zhang K, Bird J P, Wang L, Mei W-N, Hong X and Dowben P A 2017 Moving towards the magnetoelectric graphene transistor *Appl. Phys. Lett.* **111** 182402
[20] Dowben P A, Nikonov D E, Marshall A and Binek C H 2020 Magneto-electric antiferromagnetic spin-orbit logic devices *Appl. Phys. Lett.* **116** 080502

[21] Marshal A and Dowben P A 2020 Magneto-electric transistor devices and circuits with steering logic *IEEE 14th Dallas Circuits and Systems Conf. (DCAS) IEEE Explore* pp 1–4 (available at: https://ieeexplore.ieee.org/document/9330662)

[22] Angizi S, Khoshavi N, Marshall A, Dowben P and Fan D 2021 MeF-RAM: a new non-volatile cache memory based on magneto-electric FET *ACM Trans. Des. Autom. Electron. Syst.* **27** 18

[23] Marshall A and Dowben P A 2022 Magneto-electric transistor devices and circuits with steering logic in *Advances in Semiconductor Technologies: Selected Topics beyond Conventional CMOS* ed A N Chen (Hoboken, NJ: Wiley) pp 61–77

[24] Angizi S, Fan D, Marshall A and Dowben P A 2022 Non-volatile based memory architectures using magneto-electric FETs in *Advances in Semiconductor Technologies: Selected Topics beyond Conventional CMOS* ed A N Chen (Hoboken, NJ: Wiley) pp 79–92

[25] Andreev A F 1996 Macroscopic magnetic fields of antiferromagnets *JETP Lett.* **63** 758

[26] Belashchenko K D 2010 Equilibrium magnetization at the boundary of a magnetoelectric antiferromagnet *Phys. Rev. Lett.* **105** 147204

[27] He X, Wang Y, Wu N, Caruso A N, Vescovo E, Belashchenko K D, Dowben P A and Binek C 2010 Robust isothermal electric control of exchange bias at room temperature *Nat. Mater.* **9** 579–85

[28] Wu N, He X, Wysocki A, Lanke U, Komesu T, Belashchenko K D, Binek C and Dowben P A 2011 Imaging and control of surface magnetization domains in a magnetoelectric antiferromagnet *Phys. Rev. Lett.* **106** 087202

[29] Cao S *et al* 2014 Spin polarization asymmetry at the surface of chromia *New J. Phys.* **16** 073021

[30] Kosub T, Kopte M, Radu F, Schmidt O G and Makarov D 2015 All-electric access to the magnetic-field-invariant magnetization of antiferromagnets *Phys. Rev. Lett.* **115** 097201

[31] Kosub T *et al* 2017 Purely antiferromagnetic magnetoelectric random access memory *Nat. Commun.* **8** 13985

[32] Cao S, Street M, Wang J-L, Wang J, Zhang X, Binek C and Dowben P A 2017 Magnetization at the interface of Cr_2O_3 and paramagnets with large stoner susceptibility *J. Phys.: Condens. Matter* **29** 10LT01

[33] Wang J-L, Echtenkamp W, Mahmood A and Binek C 2019 Voltage controlled magnetism in Cr_2O_3 based all-thin-film systems *J. Magn. Magn. Mater.* **486** 165262

[34] Street M, Echtenkamp W, Komesu T, Cao S, Dowben A P and Binek C H 2014 Increasing the Néel temperature of magnetoelectric chromia for voltage-controlled spintronics *Appl. Phys. Lett.* **104** 222402

[35] Mahmood A *et al* 2021 Voltage controlled Néel vector rotation in zero magnetic field at CMOS-compatible temperatures *Nat. Commun.* **12** 1674

[36] Mathon J and Bergmann G 1986 Surface enhancement of palladium *J. Phys. F: Met. Phys.* **16** 887

[37] Mathon J 1986 Magnetization of a strongly paramagnetic layer in contact with a ferromagnetic substrate *J. Phys. F: Met. Phys.* **16** L217–21

[38] Mathon J 1986 Magnetisation of palladium film on nickel substrate *J. Phys. F: Met. Phys.* **16** 669

[39] Coutinho S, Edwards D M and Mathon J 1983 Magnetic moments in metallic sandwiches *J. Phys. F: Met. Phys.* **13** L143–5

[40] Schwenk D, Fishman F and Schwabl F 1988 Ferromagnetic multilayers: statics and dynamics *Phys. Rev.* B **38** 11618

[41] Dowben P A, LaGraffe D, Li D, Miller A, Zhang L, Dottl L and Onellion M 1991 Substrate induced magnetic ordering of rare earth overlayers *Phys. Rev.* B **43** 3171–9

[42] Miller A and Dowben P A 1993 Substrate induced magnetic ordering of rare earth overlayers II *J. Phys.: Condens. Matter* **5** 5459–70

[43] Ban Y, Komatsu K, Sakuragi S, Taniyama T, Kageshima H and Sato T 2018 Change in magnetization of ferromagnetic Pd(001) ultrathin films induced by the strain effect of $BaTiO_3$ *Appl. Phys. Lett.* **112** 142409

[44] Tanabe H, Sakuragi S and Sato T 2019 Manipulation of magnetization in Pd(100) ultrathin films with quantum well structure using modification of Schottky barrier potentials *App. Phys. Lett.* **114** 052404

[45] Sakuragi S, Tajiri H, Kageshima H and Sato T 2018 Spontaneous distortion via the appearance of ferromagnetism in Pd ultrathin films: observation of an inverse mechanism for the stoner criterion *Phys. Rev.* B **97** 214421

[46] Sakuragi S, Sakai T, Urata S, Aihara S, Shinto A, Kageshima H, Sawada M, Namatame H, Taniguchi M and Sato T 2014 Thickness-dependent appearance of ferromagnetism in Pd(100) ultrathin films *Phys. Rev.* B **90** 054411

[47] Toyoki K, Shiratsuchi Y, Kobane A, Mitsumata C, Kotani Y, Nakamura T and Nakatani R 2015 *Appl. Phys. Lett.* **106** 162404

[48] Echtenkamp W and Binek C 2013 Electric control of exchange bias training *Phys. Rev. Lett.* **111** 187204

[49] Wu R *et al* 2022 Magnetotransport study of van der Waals $CrPS_4$/(Pt,Pd) heterostructures: spin-flop transition and room-temperature anomalous hall effect *Phys. Rev. Appl.* **17** 064038

[50] Li Ma L *et al* 2016 Spin orbit coupling controlled spin pumping and spin hall magnetoresistance effects *Adv. Electron. Mater.* **2** 1600112

[51] Holanda J, Alves Santos O, Mendes J B S and Rezende S M 2021 Spin-to-charge conversion and interface-induced spin Hall magnetoresistance in yttrium iron garnet/metallic bilayers *J. Phys.: Condens. Matter* **33** 435803

[52] Ma L, Lang L, Kim J, Yuan Z, Wu R, Zhou S and Qiu X 2018 Spin diffusion length and spin Hall angle in Pd1−xPtx/YIG heterostructures: examination of spin relaxation mechanism *Phys. Rev.* B **98** 224424

[53] d'Allivy Kelly O *et al* 2017 Magnetic proximity effect free spin Hall magnetoresistance in YIG\Pd, special issue on spin dynamics in magnetic materials, part 2; guest editors: Mourad Chérif and Yaowen Liu *SPIN* **07** 1740005

[54] Lin T, Tang C, Alyahayaei H M and Shi J 2014 Experimental investigation of the nature of the magnetoresistance effects in Pd-YIG hybrid structures *Phys. Rev. Lett.* **113** 037203

[55] Jungwirth T, Wunderlich J and Olejník K 2012 Spin Hall effect devices *Nat. Mater.* **11** 382–90

[56] Binek C, Mahmood A and Echtenkamp W 2022 *Hall bar device for memory and logic applications* United States Patent 11,233,192

[57] Hüfner S 1995 Inverse photoemission spectroscopy *Photoelectron spectroscopy: Principles and Applications* (*Springer Series in Solid-State Sciences vol 82*) (Berlin: Springer) ch 9, pp 403–19

[58] Smith N V 1988 Inverse photoemission *Rep. Prog. Phys.* **51** 1227–94

[59] Cazaux J 1999 Mechanisms of charging in electron spectroscopy *J. Electron Spectrosc. Relat. Phenom.* **105** 155–85

[60] Cazaux J 2000 About the charge compensation of insulating samples in XPS *J. Electron Spectrosc. Relat. Phenom.* **113** 15–33

[61] Baer D R, Artyushkova K, Cohen H, Easton C D, Engelhard M, Gengenbach T R, Greczynski G, Mack P, Morgan D J and Roberts A 2020 XPS guide: charge neutralization and binding energy referencing for insulating samples *J. Vac. Sci. Technol.* A **38** 031204
[62] Onur Tasci T, Atalar E, Demirok U K and Suzer S 2008 Electrical circuit modeling of surface structures for x-ray photoelectron spectroscopic measurements *Surf. Sci.* **602** 365–8
[63] Ertas G, Demirok U K, Atalar A and Suzera S 2005 X-ray photoelectron spectroscopy for resistance-capacitance measurements of surface structures *Appl. Phys. Lett.* **86** 183110
[64] Barr T L 1989 Studies in differential charging *J. Vac. Sci. Technol.* A **7** 1677
[65] Tielsch B J, Fulghum J E and Surman D J 1996 Differential charging in XPS. Part II. Sample mounting and x-ray flux effects on heterogeneous samples *Surf. Interface Anal.* **24** 459
[66] Xiao J *et al* 2011 Surface charging at the (100) surface of Cu doped and undoped $Li_2B_4O_7$ *Appl. Surf. Sci.* **257** 3399–403
[67] Ciccacci F, Drouhin H-J, Hermann C, Houdré R and Lampel G 1989 *Appl. Phys. Lett.* **54** 632
[68] Waldfried C, McAvoy T, Welipitiya D, Komesu T, Dowben P A and Vescovo E 1998 *Phys. Rev.* B **58** 7434
[69] Komesu T, Waldfried C, Jeong H-K, Pappas D P, Rammer T, Johnston M E, Gay T J and Dowben P A 2000 *Proc. SPIE* **3945** 6–16
[70] Fallarino L, Berger A and Binek C 2015 *Phys. Rev.* B **91** 054414
[71] Choudhary R, Komesu T, Kumar P, Manchanda P, Taguchi K, Okuda T, Miyamoto K, Dowben P A, Skomski R and Kashyap A 2016 *Europhys. Lett.* **115** 17003
[72] Hulbert S L, Johnson P D and Weinert M 1986 High-resolution inverse-photoemission study of the Pd(111) surface *Phys. Rev.* B **34** 3670–3
[73] Wesner D A, Johnson P D and Smith N V 1984 Photoemission spectra and band structures of d-band metals. XI. Inverse photoemission from Pd(111) *Phys. Rev.* B **30** 501–6
[74] Cao S, Ning W U, Echtenkamp W, Lauter V, Ambaye H, Komesu T, Binek C and Dowben P A 2015 The surface stability of Cr_2O_3(0001) *J. Phys.: Condens. Matter* **27** 255003
[75] Lübbe M and Moritz W 2009 *J. Phys.: Condens. Matter* **21** 134010
[76] Rohr F, Bäumer M, Freund H J, Mejias J A, Staemmler V, Müller S, Hammer L and Heinz K 1997 *Surf. Sci.* **372** L291–7
[77] Rohr F, Bäumer M, Freund H-J, Mejias J A, Staemmler V, Müller S, Hammer L and Heinz K 1997 *Surf. Sci.* **389** 391
[78] King H W and Manchester F D 1978 *J. Phys. F: Met. Phys.* **8** 15
[79] Arblaste J W 2012 Crystallographic properties of palladium *Platin. Met. Rev.* **56** 181–9
[80] Kilian A S, Bernardi F, Pancotti A, Landers R, de Siervo A and Marais J 2014 Atomic structure of Cr_2O_3/Ag(111) and Pd/Cr_2O_3/Ag(111) surfaces: a photoelectron diffraction investigation *J. Phys. Chem.* C **118** 20452–60
[81] Vook R W 1984 Nucleation and growths of thin films *Opt. Eng.* **23** 343–8
[82] Káňa T, Hüger E, Legut D, Čák M and Šob M 2016 Magnetism and deformation of epitaxial Pd and Rh thin films *Phys. Rev.* B **93** 134422
[83] Siervo A, de Biasi E, De,Garcia F, Landers R, Martins M D and Macedo W A A 2007 Surface structure determination of Pd ultrathin films on Ru(0001): possible magnetic behavior *Phys. Rev.* B **76** 075432
[84] Sakuragi S, Tajiri H and Sato T 2015 Ferromagnetism in Pd(100) ultrathin films enhanced by distortion *Phys. Proc.* **75** 1167–71
[85] Ho Thi H, Rhim S H and Hong S C 2022 Role of quantum well in Pd(111) thin film magnetism *J. Magn. Magn. Mater.* **563** 169891
[86] Taborelli M, Allenspach R, Boffa G and Landolt M 1986 Magnetic coupling of surface adlayers: Gd on Fe(100) *Phys. Rev. Lett.* **56** 2869